ARTICLES

Formation of Normal and Reverse Bilayer Structures by Self-Assembly of Nonionic Block Copolymers Bearing Lipid-Mimetic Units

Stanislav Rangelov,*,†,‡ Mats Almgren,† Katarina Edwards,† and Christo Tsvetanov‡

Department of Physical Chemistry, University of Uppsala, Box 579, 751 23 Uppsala, Sweden, and Institute of Polymers, Bulgarian Academy of Sciences, 1113 Sofia, Bulgaria

Received: April 17, 2003; In Final Form: January 6, 2004

PEG-based diblock and triblock copolymers bearing blocks of lipid-mimetic monomer units, 1,3-didodecyloxy-2-glycidyl-glycerol (DDGG), were synthesized via anionic polymerization. They were characterized by ^{1}H nuclear magnetic resonance spectroscopy and gel permeation chromatography. The copolymers are of a higher poly(DDGG) to PEG ratio compared to related copolymers studied earlier. They self-associate both in aqueous (water) and nonaqueous (*n*-heptane) solutions. The self-assembled structures were studied by simultaneous dynamic and static light scattering. In both solvents nanoparticles with weight-average molecular weights reaching 390×10^6 were formed. Cryogenic transmission electron microscopy performed on aqueous dispersions revealed coexistence of unilamellar vesicles and fractions of multilamellar vesicles or vesicles with internal folded lamellar structures. On the basis of numerical calculations of the area per lipid anchor, formation of reversed vesicles and disks in heptane by the diblock and triblock copolymers, respectively, was suggested. The aggregates are able to solubilize large amounts of substances that are insoluble in the medium in which the aggregates are formed. At high heptane contents the close bilayer structure of the normal vesicles in water no longer exists. Upon the addition of water the dispersions of reverse vesicles or disks in heptane undergo transition from reverse bilayers to monolayer stabilized water-in-oil emulsions.

Introduction

Self-assembled structures of amphiphilic lipids offer a diversity of applications. Some of them, in particular, liposomes (lipid vesicles) are suitable for investigations of various biophysical and biochemical processes and as model biomembrane systems.[1−9] Liposomes have found important applications in drug delivery especially after the circulation time in the bloodstream was prolonged by the introduction of an appropriate amount of polymer-derivatized lipids in the bilayer membrane.[10−16] Thus, the grafted polymers, usually poly(ethylene glycol) (PEG), create a steric repulsive barrier around the liposomes which prevents them from being taken up by the host defense system.

PEG-derivatized phospholipids, referred to as PEG-lipids, are nowadays commercially available. Typical formulations use PEG-lipids of molecular weights up to 5000 and concentrations up to 10 mol %. Larger molecular weights and/or concentrations lead to transitions from bilayer vesicles to open bilayers or micelles. In an earlier paper,[17] we investigated the ability of PEG-based copolymers that, in contrast to the PEG-lipids, bear more than one lipid anchor as stabilizers of egg-phosphatidylcholine (EPC) liposomes. It was found that the maximum amount of the copolymer that can be incorporated in the EPC membrane without affecting the liposome integrity increases with increasing number of lipid anchors. The effect was examined for copolymers of a low polylipid/PEG ratio, that is, PEG molecular weight of 5000 and up to four lipid anchors. Besides their improved ability to stabilize EPC liposomes, these copolymers, as well as related copolymers with different compositions but still of a low polylipid to PEG ratio, exhibit interesting self-assembly in water.[18] In aqueous solution they self-associate into large multichain core/corona aggregates of hydrodynamic radii and molecular weights up to 70 nm and 40×10^6, respectively. The core of the particle consists of polylipid moieties in which PEG−water domains are distributed, whereas the corona is built only of PEG chains in a brush or looping conformation depending on the copolymer architecture. Their self-assembly behavior is consistent with the shape concept as expressed by the surfactant parameter.[19−21] As shown earlier,[22−26] the PEG-lipids which have a cone-shaped geometry self-associate into micelles, that is, particles of a high curvature. By increasing the number of the lipid anchors, the hydrocarbon volume of the macromolecule increases which makes the latter less conical, and accordingly, aggregates of a lower curvature tend to form.[18] Particles of a negative curvature or reverse phases are expected to be formed with a further increase of the polylipid to PEG ratio. Although many of the self-assembled aggregate structures have their counterparts in apolar solvents, self-assembly in apolar solvents has been largely neglected especially as far as reverse vesicles are concerned. Reverse vesicle are usually produced in the presence of trace amounts of water.[27−34] Spontaneous formation without addition of water has been reported as well.[32−35]

† University of Uppsala.
‡ Bulgarian Academy of Sciences.

10.1021/jp0304576 CCC: $27.50
Published on Web 05/14/2004

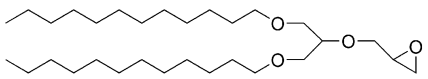

Figure 1. Chemical structure of DDGG.

A study that is concerned with two central issues regarding copolymers of higher polylipid/PEG ratios, namely, self-assembly and liposome stabilization, has been initiated. In the present contribution using static (SLS) and dynamic (DLS) light scattering as well as cryogenic transmission electron microscopy (cryo-TEM) we investigate the self-assembly in aqueous (water) and nonaqueous (*n*-heptane) solutions of diblock and triblock copolymers of 1,3-didodecyloxy-2-glycidyl-glycerol (DDGG) (see Figure 1 for the chemical structure) and ethylene oxide (EO). The copolymers investigated in the present study had considerably shorter PEG and larger poly(DDGG) moieties compared to those of related copolymers studied earlier.[17,18] We also explored the ability of the copolymer aggregates to solubilize molecules that are practically insoluble in the dispersion medium. A subsequent paper will address the properties of both EPC liposomes stabilized by the present copolymers and aggregates formed by mixing copolymers of different molecular geometry.

Experimental Section

Materials. All solvents and reagents were supplied by Fluka or Aldrich. The solvents were purified by standard methods whereas the reagents were used as received. Monohydroxy and α,ω-dihydroxy poly(ethylene glycol)s of weight-average molecular weights 2000, according to the producer (Fluka), were dried by azeotropic distillation from toluene. The monomer, DDGG, was prepared according to procedures described elsewhere.[36]

Synthesis of Block Copolymers. A 0.95 g (4.75×10^{-4} mol) sample of monohydroxy PEG 2000 previously metalled by potassium naphthalide was dissolved in 40 mL of toluene and placed in a 100 mL three-necked flask fitted with a nitrogen inlet, a reflux condenser and a rubber septum. Then, 2.3 g (4.75×10^{-3} mol) of DDGG dissolved in 5 mL of toluene was injected via a syringe. The reaction was carried out at reflux for 48 h. Then toluene was removed under reduced pressure; the residue was dissolved in methylene chloride and precipitated in hexane. A very tiny (0.028 g) hexane-insoluble fraction was isolated. Then the solvent mixture and the residual monomer were removed under reduced pressure and at high (10^{-5} Torr) vacuum, respectively. About 2.5 g of a slightly colored grease-like solid was obtained.

The synthesis of the triblock copolymer was carried out in a similar manner with a slightly different procedure including the usage of α,ω-dihydroxy PEG 2000 and a monomer-to-precursor ratio as high as 20:1.

The block structure of the resulting copolymers was proved by GPC. The GPC traces for the starting monohydroxy PEG 2000 and the resulting diblock copolymer are presented in Figure 2. The polydispersity index, also determined by GPC, for the triblock copolymer was slightly higher than that of the diblock copolymer—1.19 and 1.14, respectively. The ^{1}H NMR spectra of the present copolymers are qualitatively similar to those shown earlier[18,26,36] and therefore not presented. The compositions of the copolymers were determined from the ^{1}H NMR data assuming a degree of polymerization of the PEG moieties of 45. They are as follows: $(EO)_{45}(DDGG)_8$ and $(DDGG)_7$-$(EO)_{45}(DDGG)_7$. The compositions determined from the ^{1}H NMR, GPC, and material balance of the reaction are in good agreement.

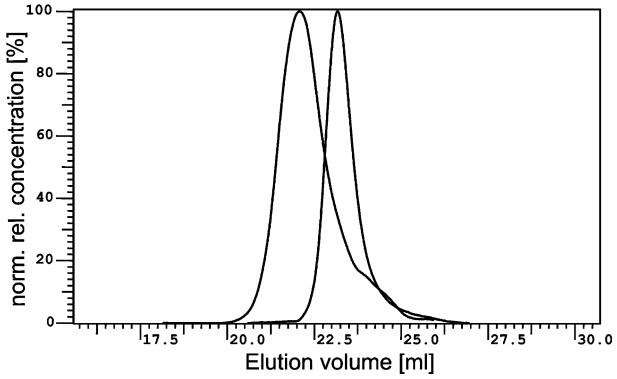

Figure 2. GPC curves of the monohydroxy PEG 2000 precursor (right) and the resulting diblock copolymer (left).

Preparation of Dispersions. Heptane dispersions in a wide concentration range were prepared by adding heptane to weighed amounts of a dry bulk copolymer. The samples were kept overnight at room temperature and then stirred with a magnetic stirrer for a couple of hours and filtered directly into dust-free light scattering cells using 0.2 μm pore-size inorganic filters (Whatman). The aqueous dispersions were prepared according to a method known to yield vesicles of synthetic and natural lipids.[37−39] Purified water provided by Millipore Super-Q-System was added to a dry copolymer film cast from a solution in chloroform. The resulting dispersions were subjected to eight freeze−thaw cycles and then extruded 30 times through polycarbonate filters of pore size 200 nm.

Solubilization. The solubilizates were added as portions of 1−2 μL to dispersions of the copolymers with a total volume 1 mL and concentrations 8.0 and 0.114 mg/mL in heptane and water, respectively. After the addition of each portion, the samples were agitated intensively by vigorous hand shaking for about 15 min Afterward, they were kept at room temperature for at least 30 min and then measured. Static and dynamic light scattering measurements were carried out at a single concentration, 25 °C and various angles between 50° and 130°. The ultimately derived hydrodynamic radii and radii of gyration are thus apparent radii at a finite concentration.

Methods. *Nuclear Magnetic Resonance (NMR).* ^{1}H NMR spectra were recorded at 250 MHz on a Bruker 250 spectrometer. The samples were prepared as solutions in $CDCl_3$ or DMSO. All spectra were recorded at 25 °C.

Gel Permeation Chromatography (GPC). The GPC system (Waters) consisted of four styragel columns with nominal pore sizes of 100, 500, 500, and 1000 Å, eluted with tetrahydrofuran at 40 °C. The flow rate of the eluent was 1 mL/min. Samples were prepared as solutions in tetrahydrofuran. Elution volumes were referenced to toluene as internal standard. Calibration was done with PEG standards and derived weight-average molar masses and degrees of polymerization were determined as if samples were PEG.

Cryogenic Transmission Electron Microscopy (cryo-TEM). Transmission electron microscopy observations were conducted on a Zeiss EM 902 A instrument operating at 80 kV. The procedure for the sample preparation is described in the following. A drop of the dispersion is deposited on an electron microscopy copper grid coated by a perforated polymer film. The excess of the liquid is blotted by a filter paper, leaving a thin film of the dispersion on the grid. The above operations are performed in a special chamber where the environmental conditions (constant temperature and high humidity) are under strict control. The film on the grid is vitrified by plunging the

TABLE 1: Refractive Index Increment (d*n*/d*c*) Values in mL/g for $(EO)_{45}(DDGG)_8$ and $(DDGG)_7(EO)_{45}(DDGG)_7$ in Water and Heptane at 25 °C

	$(EO)_{45}(DDGG)_8$	$(DDGG)_7(EO)_{45}(DDGG)_7$
water	0.107	0.109
heptane	0.074	0.078

grid into liquid ethane held at temperature below 100 K. Because of the rapid cooling of the aqueous film vitreous ice is formed. The vitrified sample is then transferred to the microscope for observation. During observation and transfer the temperature is kept below 100 K.

Light Scattering. The light scattering setup consists, as described previously,[40] of a 488 nm Ar ion laser and the detector optics with an ITT FW 130 photomultiplier and ALV-PM-PD amplifier−discriminator connected to an ALV-5000 autocorrelator built into a computer. The cylindrical scattering cells were sealed and then immersed in a large-diameter thermostated bath containing the index matching fluid decalin. Measurements were made at different angles in the range 50−130° and at different concentrations. Information on the molecular weight, the radius of gyration, and the second virial coefficient was obtained from the static light scattering data using the Zimm plot method. The angular dependence of the reduced scattered intensity, Kc/R_θ, of a number of copolymer solutions was measured in the simultaneous static and dynamic experiments. Here $K = (4\pi^2 n^2/N_A\lambda^4)(dn/dc)^2$, N_A is Avogadro's constant, and λ the wavelength of the light in a vacuum. The refractive index increment (dn/dc) was measured in a differential refractometer with Rayleigh optics. dn/dc values for the present copolymers are collected in Table 1. The Rayleigh ratio was determined as $R_\theta = [(I - I_o)/I_{ref}]R_{ref}(n/n_{ref})^2$. Here n is the solvent refractive index and n_{ref} that of toluene. I is the measured total time-average scattered intensity, I_o that of the solvent, and I_{ref} that of toluene. Toluene was used as the reference scatterer ($R_{ref} = 4.0 \times 10^{-3}$ m^{-1} at $\lambda = 488$ nm[40]). The reduced scattered intensity was either linearly dependent on $\sin^2(\theta/2)$ or just slightly curved at higher angles indicating that the angle range was appropriately chosen. Here θ is the scattering angle.

Analysis of the dynamic data was performed by fitting the experimentally measured $g_2(t)$, the normalized intensity autocorrelation function, which is related to the electrical field correlation function $g_1(t)$ by the Siegert relationship[41]

$$g_2(t) - 1 = \beta\,|g_1(t)|^2 \tag{1}$$

where β is a factor accounting for deviation from ideal correlation. For polydisperse samples, $g_1(t)$ can be written as the inverse Laplace transform (ILT) of the relaxation time distribution, $\tau A(\tau)$

$$g_1(t) = \int \tau A(\tau)\exp(-t/\tau)\,d(\ln\tau) \tag{2}$$

where t is the lag-time. The relaxation time distribution, $\tau A(\tau)$, is obtained by performing ILT using the constrained regularization algorithm REPES,[42] which minimizes the sum of the squared differences between the experimental and calculated $g_2(t)$. A mean diffusion coefficient D is calculated from the second moment of each peak as $D = \Gamma/q^2$, where q is the magnitude of the scattering vector $q = (4\pi n/\lambda)\sin(\theta/2)$ and $\Gamma = 1/\tau$ is the relaxation rate of each mode. Here θ is the scattering angle, n the refractive index of the medium, and λ the wavelength of the light in a vacuum.

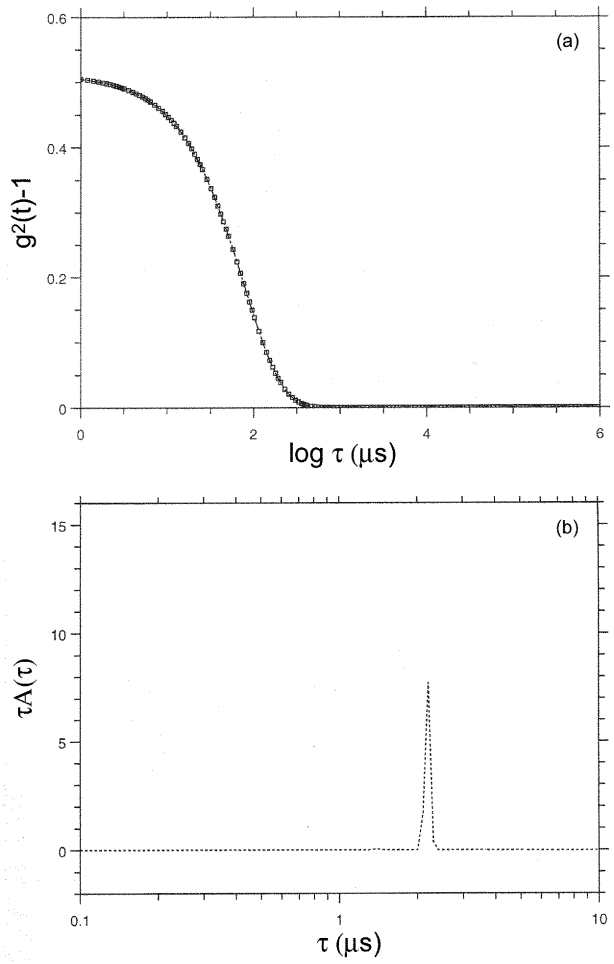

Figure 3. (a) Autocorrelation function for $(EO)_{45}(DDGG)_8$ in heptane at $c = 9.0$ mg/mL, angle 90°, and 25 °C. (b) Corresponding relaxation time distribution data in part a.

Within the dilute regime, D varies linearly with the concentration according to

$$D = D_o(1 + k_D C + ...) \tag{3}$$

where D_o is the diffusion coefficient at infinite dilution and k_D is the hydrodynamic "virial" coefficient.

The Stokes−Einstein equation relates D_o to the hydrodynamic radius (R_h):

$$R_h = kT/(6\pi\eta D_o) \tag{4}$$

kT is the thermal energy factor and η is the temperature-dependent viscosity of the solvent.

Results and Discussion

LS Parameters. SLS and DLS experiments were performed simultaneously on dispersions of the block copolymers in heptane and water in a wide concentration range. Heptane and water are nonsolvents for the PEG moiety and lipid anchors, respectively, and thus the copolymers are expected to self-associate when dispersed in any of the above solvents.

Examples of an autocorrelation function and the corresponding relaxation time distribution function are presented in Figure 3, parts a and b, for the diblock copolymer in heptane at $c = 9.0$ mg/mL and 25 °C. The autocorrelation function for both copolymers were single-exponential and the distributions monomodal. The peaks in the investigated concentration intervals

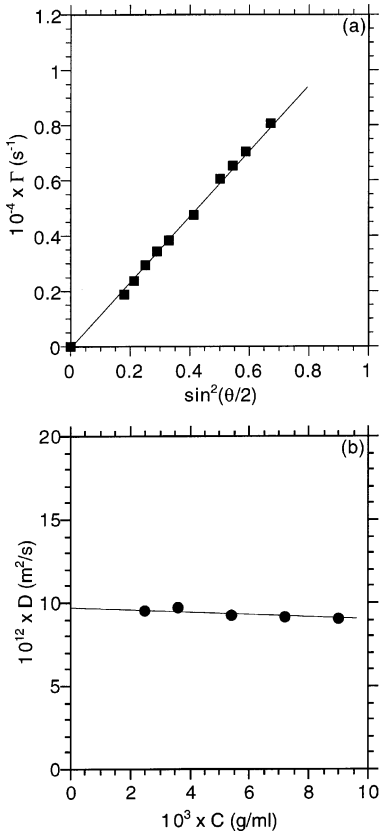

Figure 4. (a) Relaxation rate (Γ) as a function of $\sin^2(\theta/2)$ for $(EO)_{45}$-$(DDGG)_8$ in heptane at $c = 2.5$ mg/mL and 25 °C. (b) Concentration dependence of the diffusion coefficients for $(EO)_{45}(DDGG)_8$ in heptane. The lines through the data points represent the linear fits to the data.

were diffusive as demonstrated in Figure 4a where the relaxation rates are plotted as a function of $\sin^2(\theta/2)$. The diffusion coefficients were determined from the slopes of the linear fit to the data, then plotted against concentration and extrapolated to zero concentration (Figure 4b). The values of D_o, extrapolated to zero concentration were used to calculate the particle hydrodynamic radius, R_h (eq 4). D_o and R_h for both copolymers are collected in Table 2.

SLS experiments were performed simultaneously with DLS. The measurements were made in the concentration ranges 2.5−9.0 and 12.0−20.0 mg/mL for the diblock and triblock copolymers, respectively, at nine angles between 50 and 130.° Weight-average molecular weights, M_w, radii of gyration, R_g, and second virial coefficients, A_2, were calculated using a Zimm plot method. A typical Zimm plot is shown in Figure 5, and the SLS parameters are collected in Table 2.

The copolymers are less soluble in water than in heptane. Therefore, to obtain stable dispersions and reproducible results, the initial aqueous dispersions were subjected to eight freeze−thaw cycles and then extruded 30 times through polycarbonate filters of pore size 200 nm. The LS results of the aqueous dispersions are summarized in Figures 6−8, and the LS parameters are listed in Table 3. As seen, there are a number of similarities between the results from the nonaqueous and aqueous dispersions: monomodal relaxation time distribution (Figure 6b); an almost perfect linear dependence of the

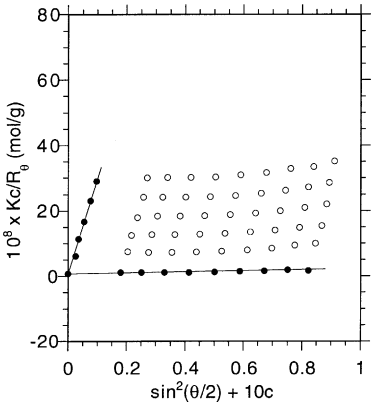

Figure 5. Zimm plot of $(EO)_{45}(DDGG)_8$ in heptane at 25 °C: experimental points (open symbols); extrapolated points to zero concentration and zero scattering angle (filled symbols).

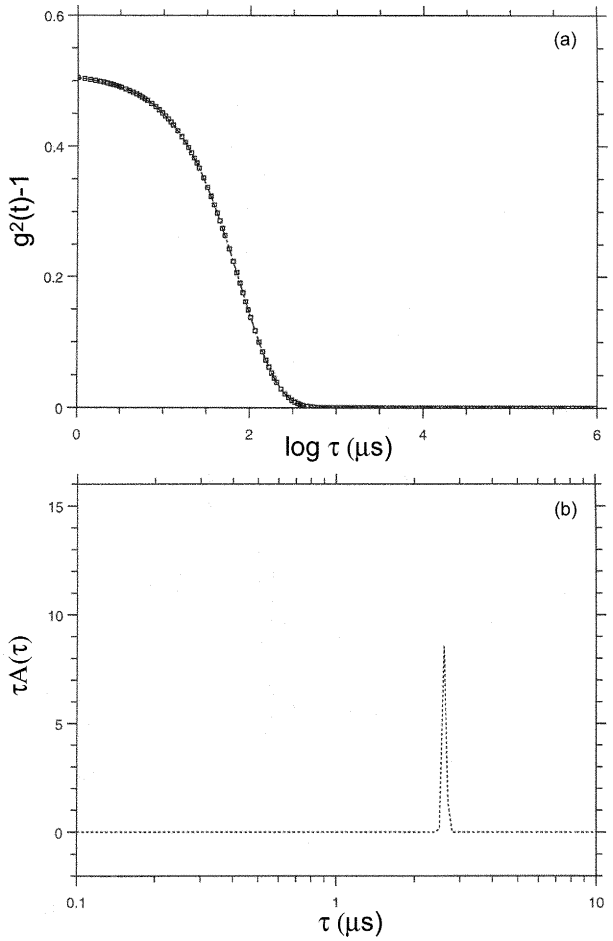

Figure 6. (a) Autocorrelation function for $(EO)_{45}(DDGG)_8$ in water at $c = 0.38$ mg/mL, angle 90°, and 25 °C. (b) Corresponding relaxation time distribution data in part a.

relaxation rate on $\sin^2(\theta/2)$, satisfying the equation $\Gamma = Dq^2$ (Figure 7a); a weak concentration dependence (Figure 7b) with a slightly negative hydrodynamic virial coefficient, k_D (eq 3). There is only a slight curvature in the dependence of the reduced scattered intensity on $\sin^2(\theta/2)$ (Figure 8) that could be attributed to the higher radii of gyration in the aqueous than in the

TABLE 2: Static and Dynamic Light Scattering Parameters of the Copolymers in Heptane at 25 °C

copolymer	$10^{-6}M_w$	10^6A_2 (mol·mL/g^2)	R_g (nm)	$10^{12}D_o$ (m^2/s)	R_h (nm)	R_g/R_h
$(EO)_{45}(DDGG)_8$	126.8	1.55	60.5	9.88	57.2	1.06
$(DDGG)_7(EO)_{45}(DDGG)_7$	4.77	18.73	45.9	14.05	40.2	1.14

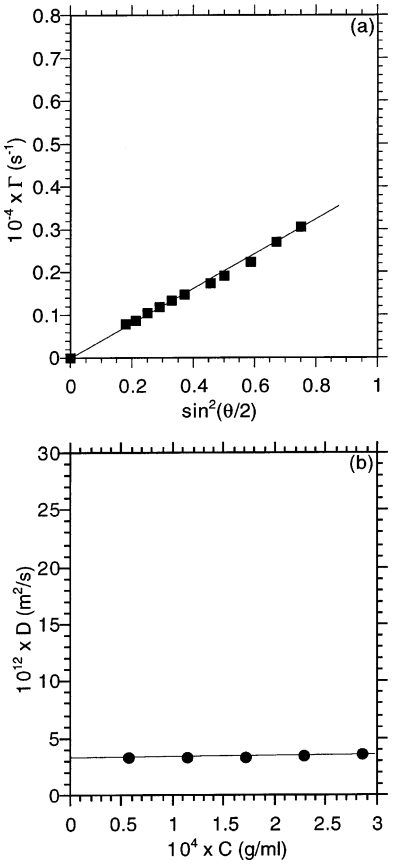

Figure 7. (a) Relaxation rate (Γ) as a function of $\sin^2(\theta/2)$ for $(DDGG)_7(EO)_{45}(DDGG)_7$ in water at $c = 0.171$ mg/mL and 25 °C. (b) Concentration dependence of the diffusion coefficients for $(DDGG)_7(EO)_{45}(DDGG)_7$ in water. The lines through the data points represent the linear fits to the data.

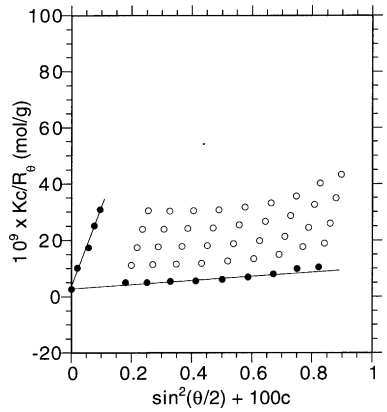

Figure 8. Zimm plot of $(EO)_{45}(DDGG)_8$ in water at 25 °C: experimental points (open symbols); extrapolated points to zero concentration and zero scattering angle (filled symbols).

nonaqueous surrounding. The nonlinearity, although not strictly observed, in the angle dependence is anticipated when large particles are present and the product $qR_g < 1$ may no longer hold at higher angles.

Particles with hydrodynamic radii in the range 40−70 nm and weight-average molecular weights up to hundreds of millions (Tables 2 and 3) are formed both in heptane and water. The second virial coefficients in both solvents are very low (10^{-5}−10^{-6} mol·mL/g^2). In heptane the M_w value of the diblock copolymer is comparable to that in water, whereas for the triblock copolymer it is 2 orders of magnitude lower than the corresponding value in water. The value of 4.77×10^6 for $(DDGG)_7(EO)_{45}(DDGG)_7$ in heptane is consistent with the small dimension of the particles.

Particle Structure. An important question to be clarified is how the macromolecules are arranged in the self-assembled structures in water and heptane. In a selective solvent the amphiphilic block copolymers associate into large multichain particles that presumably consist of microdomains in which the less soluble moieties are gathered, stabilized by the more soluble segments that interact with the solvent. Clearly, the particles are too large to be simple micelles, that is, of core/corona morphology since even the fully stretched macromolecule is not long enough to span a diameter of 80 nm or more. In addition, the shape concept[19−21] does not favor such an arrangement. On the basis of simple geometrical considerations this concept relates the shape of the surfactant molecules to the type of the aggregate morphology. Accordingly, "cone-shaped" molecules, that is with a large hydrophilic part, self-associate into micelles, whereas lamellae or bilayers are the preferred aggregate structures of molecules with a "cylindrical shape", i.e., with similar volumes of the hydrophilic and hydrophobic parts. With their larger hydrocarbon volumes and smaller PEG sizes compared to those of the copolymers studied earlier,[18,26,36] the present copolymers are expected to form aggregates with low curvature.

Cryo-TEM was employed to visualize the aggregates obtained in aqueous solution. This technique has opened the possibility for direct imaging of structures formed by amphiphilic molecules in aqueous environments.[43,44] Unfortunately, it is not easily applicable to nonaqueous solutions. Clearly, the particles shown in Figure 9 are vesicles. Contrary to the DLS results large clusters of aggregated vesicles seem to dominate the samples (Figure 9, parts a and c). Such huge clusters would be easily detected by DLS, but were not observed, not even in the noncentrifuged solutions. This implies that the clustering takes place during the preparation of the samples for microscopy; it may be an effect from the confinement in a thin film. As seen from Figure 9 not all vesicles are unilamellar, although the latter are the majority. Also, there is a fraction of irregular particles consisting of two different parts (Figure 9b). One has a regular bilayer structure and the other represents folded structures with numerous interlamellar connections. Dark spherical objects (arrows in Figure 9b) similar to those observed earlier[18] were detected as well. We also documented perfectly spherical, nonaggregated, and well-separated vesicles (Figure 9d). Their dimensions correspond well with the results from the DLS.

From the DLS and SLS results, we may calculate the mean area occupied per polymer, assuming that all aggregates are single wall vesicles. From the radius measured by DLS we get the total area of the vesicular bilayer, and from SLS we get the molar mass of the vesicles or their aggregation number. Such calculations for the aqueous dispersions give consistently very low values of the area available per polymer, much lower than

TABLE 3: Static and Dynamic Light Scattering Parameters of the Copolymers in Water at 25 °C

copolymer	$10^{-6}M_w$	10^6A_2 (mol·mL/g^2)	R_g (nm)	$10^{12}D_o$ (m^2/s)	R_h (nm)	R_g/R_h
$(EO)_{45}(DDGG)_8$	386.9	3.24	73.6	4.00	61.3	1.20
$(DDGG)_7(EO)_{45}(DDGG)_7$	275.9	21.5	78.5	3.50	70.0	1.12

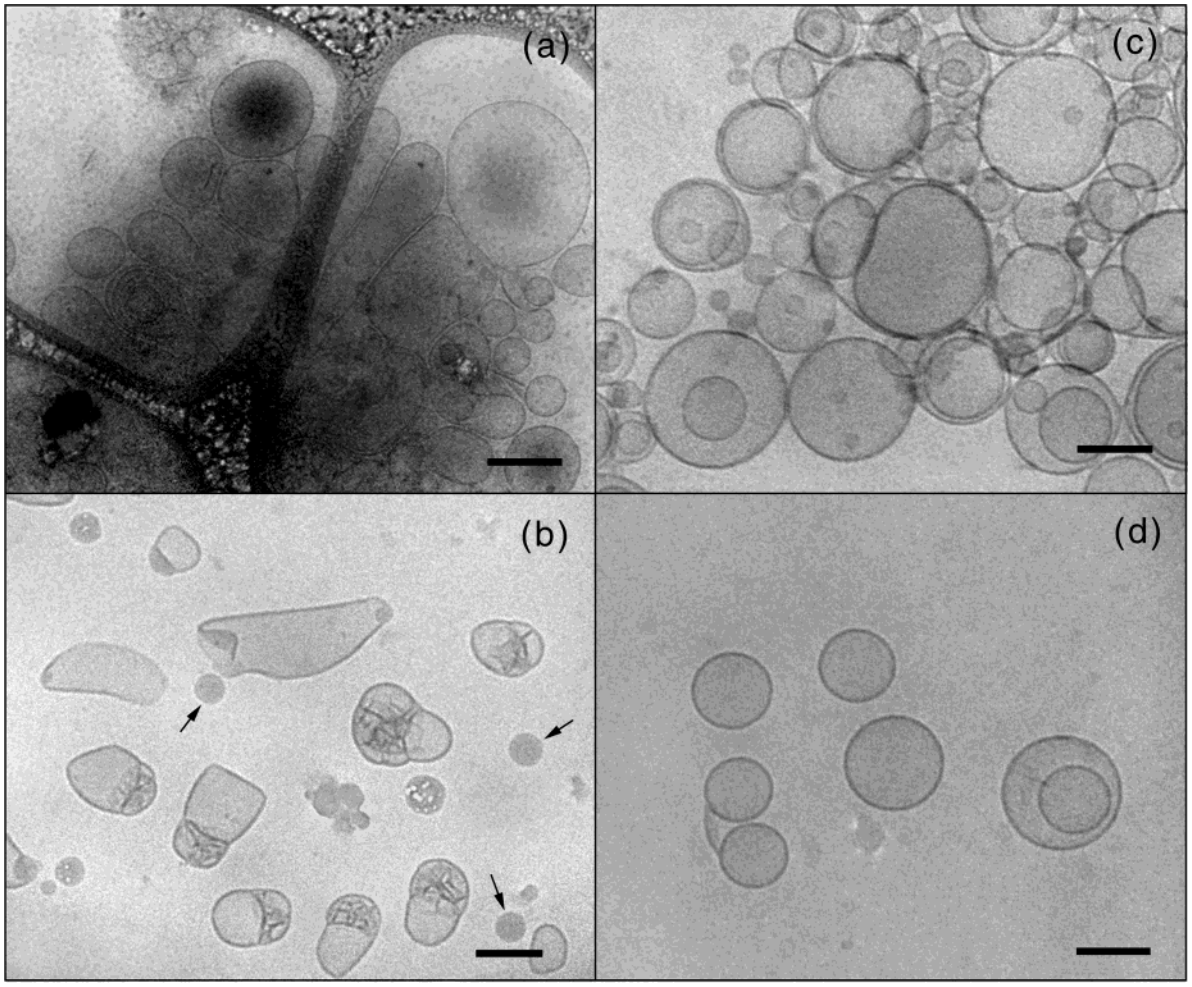

Figure 9. Cryo-TEM micrographs of vesicles taken from water dispersions of $(DDGG)_7(EO)_{45}(DDGG)_7$ (a and b) and $(EO)_{45}(DDGG)_8$ (c and d). Bar = 500 nm in part a and 100 nm in parts b−d. Arrows in part b denote dark spherical objects. Concentrations: 0.725 and 0.285 mg/mL for $(EO)_{45}(DDGG)_8$ and $(DDGG)_7(EO)_{45}(DDGG)_7$, respectively.

what is physically reasonable. The reason may be that there is a fraction of multilamellar vesicles as well as vesicles with internal structure. Also, a broad polydispersity in particular with a large fraction of the total mass in small aggregates (there is no such indication in the light scattering results, however) can make the estimated area too small.

Using the DLS and SLS results (Table 2) and applying the same simple calculations for $(EO)_{45}(DDGG)_8$ in heptane, the mean area per anchor was obtained as 0.47 nm^2, which is a possible value, consistent with the formation of reverse vesicles in heptane. The calculations made for $(DDGG)_7(EO)_{45}(DDGG)_7$ in heptane, however, gave an unrealistic high value of 5.33 nm.[2] As shown above, the formation of spherical core/corona micelles is unlikely. The formation of other micellar structures, e.g. cylindrical micelles, can also be ruled out since the R_g/R_h ratio for the present system is close to unity instead of being higher than 2 as is typical for cylinders.[45,46] An alternative bilayer organization that permits an optimal anchor area to be realized is the disklike structure. The combination of dynamic and static light scattering measurements yields the quantity R_g/R_h which has distinctly different values for different particle shapes and therefore provides useful information about the particle geometry.[45,46] For monodisperse infinitely thin disks $R_g/R_h \approx 0.943$;[46] a finite thickness gives a smaller value. On the other hand, the ratio is also sensitive to polydispersity of the particles and increases with increasing polydispersity. The value of R_g/R_h for $(DDGG)_7(EO)_{45}(DDGG)_7$ in heptane is slightly larger than 0.943 (Table 2) which is consistent with thin polydisperse disk structures. Assuming a disklike arrangement it turns out that the hydrodynamic radius derived from DLS is not identical with the radius of the disk, since the former was calculated from the equation of Stokes−Einstein (eq 4) assuming a spherical shape of the particles. A number of studies[46−54] deal with the interrelations that connect the form factor, mean square radius of gyration, hydrodynamic radius, and second virial coefficient for various structural models with the characteristic parameters of the corresponding structures, e.g., a radius and thickness of a disk or persistence length of polymer-like micelles. Equation 5 relates the apparent hydrodynamic radius measured in DLS experiments with the radius, R, and thickness, d, of a disk.[54]

$$R_h = 3R/2[(1 + d^2/4R^2)^{1/2} + (2R/d)\ln(1 + d^2/4R^2)^{1/2}]^{-1} \quad (5)$$

To calculate R an estimation of the disk thickness has to be made. The length of a fully extended C_{12} aliphatic chain is about 1.7 nm.[55] In addition the PEG layer thickness should be taken into account, since the PEG heads are larger than the hydrophilic heads of the conventional lipids. In the absence of water, the PEG chains are collapsed; the thickness of the PEG interior was calculated to be 1.5 nm (see below for the precise calculations). On the basis of the above estimations we can conclude that the disk thickness should not exceed 5 nm. Assuming values of d in the 3−5 nm range and using the

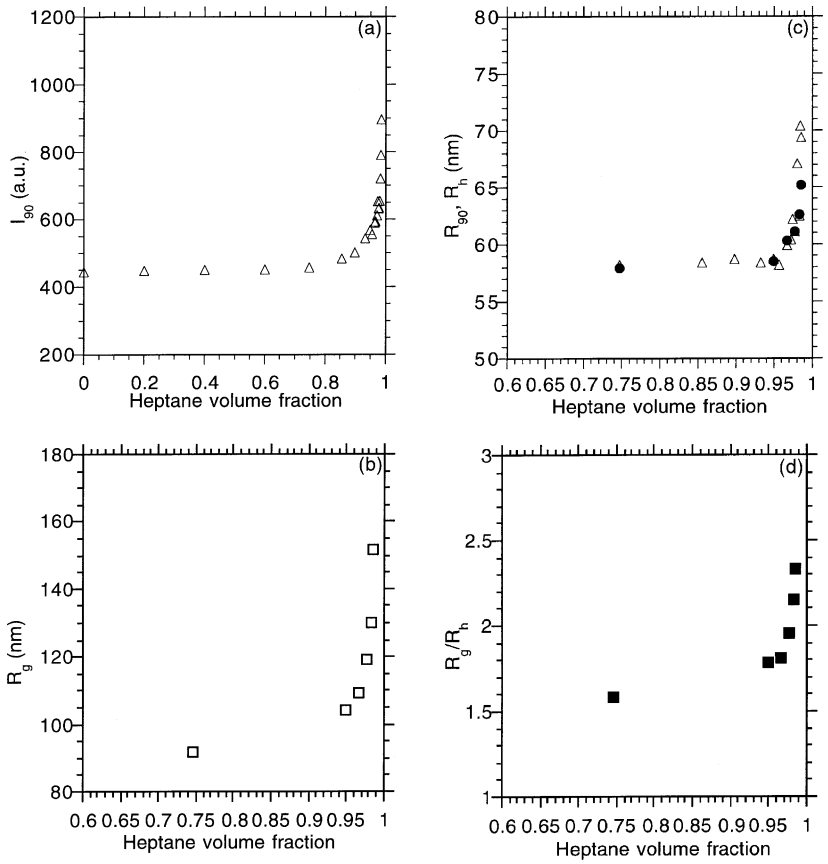

Figure 10. Variations of (a) scattered light intensity at 90°, I_{90}, (b) radius of gyration measured at $c = 0.114$ mg/mL, R_g, (c) hydrodynamic radius at 90°, R_{90} (open triangles) and hydrodynamic radius at $c = 0.114$ mg/mL extrapolated to zero scattering angle, R_h (filled circles), and (d) R_g/R_h ratio for $(EO)_{45}(DDGG)_8$ in water with the heptane volume fraction.

apparent value of the hydrodynamic radius of 40.2 nm (Table 2), eq 5 results in R values of about 27.5−28 nm, which in turn gives a lipid anchor area in the reasonable range 0.62−0.64 nm.[2] In the triblock copolymer the PEG block is placed between two poly(DDGG) blocks and probably requires more space than when one end is free. That may be why the resulting anchor area for $(DDGG)_7(EO)_{45}(DDGG)_7$ is slightly larger than that of $(EO)_{45}(DDGG)_8$ (value of 0.47 nm^2).

In short, $(EO)_{45}(DDGG)_8$ and $(DDGG)_7(EO)_{45}(DDGG)_7$ were shown to from bilayer structures in both aqueous and nonaqueous continuous media. These are mainly closed bilayer vesicles in water and reverse vesicles and disks in heptane.

Solubilization Ability. One of the most useful properties of aggregates made of amphiphilic copolymers is their ability to incorporate substances that are sparingly soluble or even insoluble in the medium in which the aggregates are formed. This phenomenon is referred to as solubilization. During this process, the solubilizate is incorporated in the solvent-insoluble microenvironment of the aggregate. Compared to conventional low molecular weight surfactant micelles, the block copolymer micelles have larger solubilization capacity. This has been demonstrated for solubilization of hydrocarbons in aqueous solutions of poly(ethylene oxide)−poly(propylene oxide) and poly(vinylpyrrolidone)−poly(styrene) block copolymers.[56] As predicted on the basis of a simple molecular theory of solubilization,[57] the solubilization capacity increases as we move from core/corona spherical to cylindrical and then to lamellar aggregates. Furthermore, the predictions show that the solubilization capacity is large when the insoluble block core/solubilizate interactions are favorable, the solubilizate-solvent interfacial tension is low, and the molecular volume of the solubilizate is small.[57] Having in mind the lamellar organization of the particles and the above considerations, enhanced solubilization capacity of the present copolymers can be expected. In this section the ability of the aggregates of the present copolymers to solubilize practically insoluble substances is examined. The amounts of the solubilized substance are expressed as volume fractions in the aggregates, i.e., the ratio of the volume of the solubilizate to the total volume of the solubilizate and the copolymer. The molecular volumes, which were used to calculate the volume fractions were taken either from the literature[57] (for the solubilizates) or calculated using literature data for the volumes of the component groups[58] (for the copolymers).

Heptane Solubilization in Aqueous Solution. The aqueous solutions of the two copolymers showed similar behavior during heptane solubilization. The DLS relaxation time distributions were predominantly monomodal: low amplitude (less than 8%) fast or slow modes appeared only occasionally; their amplitudes and frequency of appearance did not vary systematically and did not influence appreciably the main results. Figure 10 summarizes the effect of heptane addition as monitored by static and dynamic light scattering. It is evident that the scattered light intensity at 90° (I_{90}), the radius of gyration measured at a finite concentration (R_g), the hydrodynamic radius measured at 90° (R_{90}), and the hydrodynamic radius at a finite concentration extrapolated to zero scattering angle (R_h) all exhibit similar dependences upon heptane addition. No change in the above parameters was observed until the heptane volume fraction reached a value as high as 0.75 (Figure 10a−c). With further heptane addition the values of all parameters increased sharply. At the highest heptane contents, corresponding to heptane

volume fractions 0.985 and 0.975 for the diblock and the triblock copolymer, respectively, the systems were no longer homogeneous, setting an upper limit of the solubilization capacity of the copolymers. Although qualitatively similar, the quantitative dependencies of R_h and R_g differ (Figure 10, parts b and c), which results in variations of the R_g/R_h ratio (Figure 10d). The curve pattern in Figure 10d is similar to those for I_{90}, R_{90}, R_h, and R_g, i.e., an exponential increase at high heptane volume fraction. As seen, in the absence of heptane, R_g/R_h increases from 1.20, a value which is consistent with large polydisperse unilamellar vesicles, to values higher than 2 at high heptane contents. Values of $R_g/R_h > 2$ are characteristic of rodlike particles.[45,46] Thus, the observed variation of R_g/R_h suggests a shape transformation from closed vesicles to elongated structures upon heptane addition. Structures found in cryo-TEM investigations are shown in Figure 11. The images are taken from aged dispersions with the highest heptane content, i.e., close to macrophase separation. A striking result is that no vesicles were found. Some of the material appears to be in the form of elongated bilayer flakes observable both face-on and edge-on, which is consistent with the R_g/R_h increase. The large nonlamellar aggregates in Figure 11 are difficult for interpretation since there were no indications for such large particles in the light scattering results. On the other hand, however, the existence of large particles explains the solubilization of so much heptane. Obviously, the objects in Figure 11 are intermediate structures since formation of heptane droplets stabilized by a monolayer of copolymer is eventually expected.

In summary, the copolymers are able to solubilize large amounts of heptane. During the solubilization, heptane is presumably accommodated in the hydrophobic environment offered by the bilayer interior. At high heptane contents major rearrangements take place transforming the closed vesicle structures into elongated flakes and other structures.

Water Solubilization in Heptane Solution. The effects of water solubilization in reverse vesicles or disks formed in heptane by $(EO)_{45}(DDGG)_8$ and $(DDGG)_7(EO)_{45}(DDGG)_7$, respectively, were monitored using static and dynamic light scattering. The addition of water induces much more dramatic changes in the light scattering parameters than the addition of heptane to dispersions of normal vesicles in water. Although the two copolymers form different types of aggregates in heptane, the variations of the parameters were similar, which implies that the underlying events that take place upon water solubilization are the same. The results are summarized in Figures 12 and 13.

Figure 12 shows the variations of the scattered light intensity at an angle 90°, I_{90}, with the water volume fraction for the diblock copolymer. Addition of a small quantity of water, corresponding to a water volume fraction of about 0.1, causes an abrupt decrease in I_{90}. Up to a water volume fraction of about 0.4, the addition of water has no further effect on I_{90} which remains constant and low. With a further increase of the water content, however, the intensity increases sharply, reaches maximum at 0.52 for $(EO)_{45}(DDGG)_8$ and 0.45 for $(DDGG)_7(EO)_{45}(DDGG)_7$ and then decreases most probably due to the multiple scattering, since the dispersions become milky-white opalescent.[18,59]

The evolution of the relaxation time distribution upon water solubilization for the triblock copolymer is shown in Figure 13. It is evident that the addition of very small amounts of water causes dramatic changes in the relaxation time distribution which is no longer monomodal. The distribution is bimodal in the whole interval of low scattered light intensity. Both modes are proportional to q^2, satisfying the equation $\Gamma = Dq^2$ (not shown).

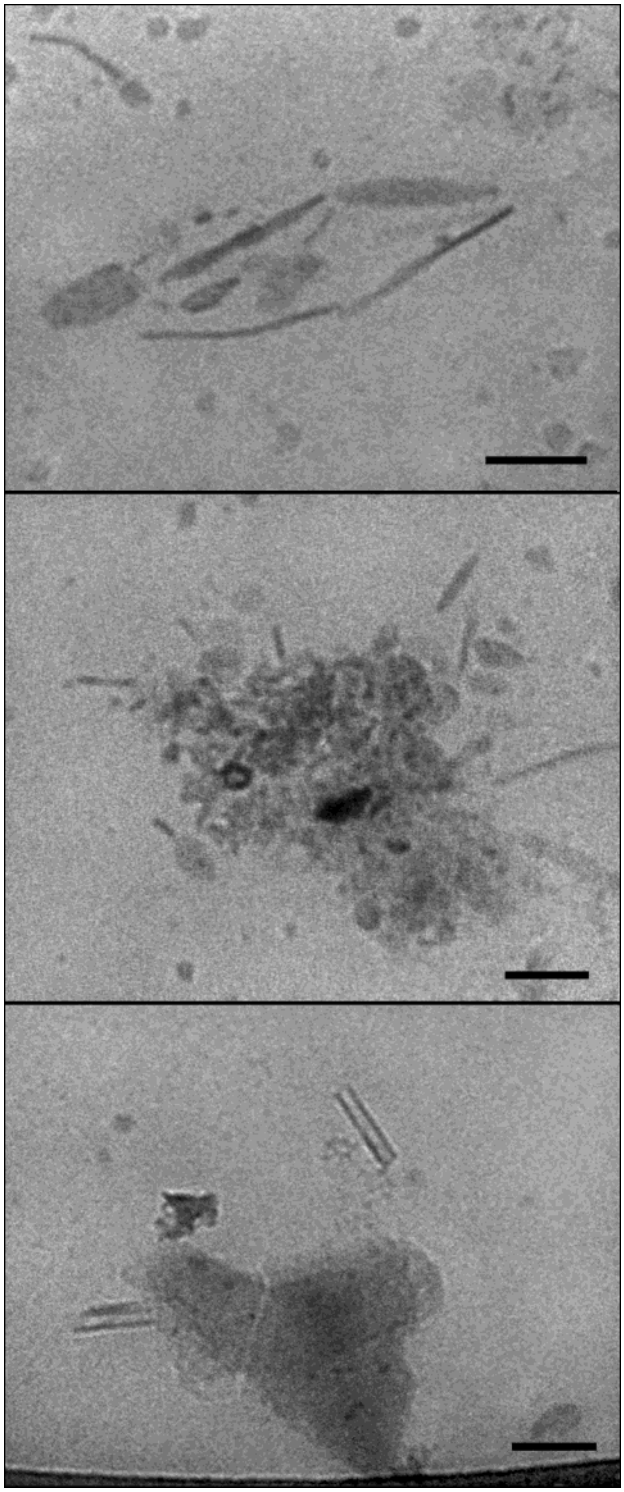

Figure 11. Elongated bilayer fragments observable at high (up to 0.8 v. %) heptane contents upon heptane solubilization by normal vesicle in water. $C_{copolymer} = 0.114$ mg/mL. Bar = 100 nm.

The position of the slow mode practically does not change from its initial position in the absence of water (the bottom curve in Figure 13) which indicates that the slow mode corresponds to the initial reverse lamellar particles. Its amplitude, however, is found to decrease with increasing water volume fraction. The new modes are invariably faster than those attributed to the lamellar particles. They are, however, slowed progressively with increasing water volume fraction and correspond to particles with hydrodynamic radii from several to tens of nanometers, i.e., much larger than usually found for w/o microemulsion

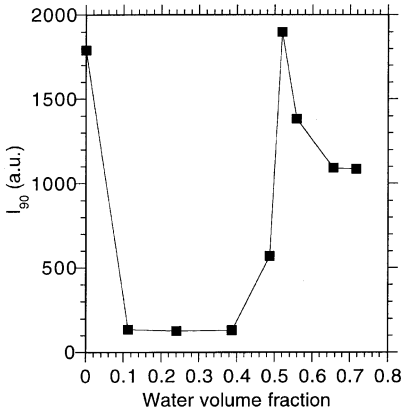

Figure 12. Variations of scattered light intensity at 90°, I_{90} of $(EO)_{45}$-$(DDGG)_8$ in heptane at $c = 8.0$ mg/mL with the water volume fraction.

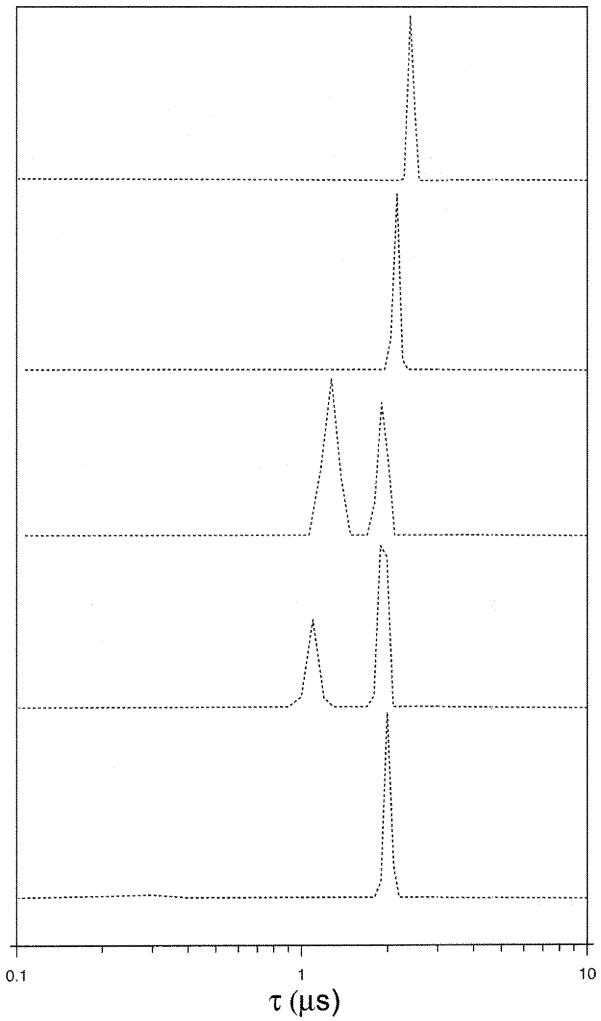

Figure 13. Variations of the relaxation time distributions with water volume fraction measured at 90° and 25 °C for $(DDGG)_7(EO)_{45}$-$(DDGG)_7$ in heptane at $c = 8.0$ mg/mL. Water volume fractions from bottom to top: 0; 0.106; 0.228; 0.371; 0.541.

particles. The fraction of these particles increases as evidenced from the increasing amplitudes of the fast modes. In the interval where an abrupt increase of I_{90} occurs the single mode behavior is manifested again. The position of the mode is constantly moved toward longer relaxation times and, accordingly, the dimensions of the particles are found to increase with increasing water volume fraction reaching 120−150 nm in radius at the onset of the multiple scattering. It is noteworthy that it is the multiple scattering that sets the upper limit of the investigation of water solubilization. The highest values of the water volume fraction that can be deduced from Figures 12 and 13 do not necessarily represent the maximal solubilization capacities of the copolymers before macrophase separation occurs.

To explain the nature of the basic events taking place during the process of water solubilization, we should go back to the model of the molecular arrangement in the reverse vesicles and disks and estimate more precisely the thickness of the PEG interior. As shown above, the PEG chains in the interior of the bilayer are collapsed and packed between the two monolayers (Figure 14a). We can calculate the volume of the PEG using literature data for the volume of the EO unit[57] and experimental data for the degree of polymerization of the PEG block and the copolymer aggregation number of the particles. The resulting volume is subtracted from the volume of a sphere with a radius R_h, which is obtained from DLS. The difference gives a volume of a sphere from which the radius can be calculated. From the difference between the two radii, the thickness of the PEG interior was calculated to be 1.5 nm. In other words, the PEG chains of all macromolecules that build up the reverse vesicle are compressed into a layer with a thickness of only 1.5 nm in which water may be solubilized. In a good solvent regime (water is a good solvent for PEG), the polymer chains expand due to repulsive intramolecular interactions. The coil dimension increases on addition of water, until maximum expansion is reached in the isolated state (infinite dilution). Consequently, during the solubilization of water the reverse bilayer is subjected to high perturbations and structural changes due to the expansion of the PEG chains. The sequence of the basic events upon water solubilization is schematically presented in Figure 14. The PEG chains interact not only with their neighbors but also with PEG chains grafted on the opposite monolayer which contributes to an increased free energy. Transformation into emulsion, or possibly microemulsion, particles, as shown in Figure 14b, could be thermodynamically favorable since such rearrangements would decrease the free energy of the system. Initially, the emulsion particles are small in size and coexist with intact reverse vesicles. This is consistent with the bimodal distribution and the sharp fall of the scattered light intensity detected in the LS experiments. On uptake of more water, the small particles tend to increase in size by coalescence. This is seen in the relaxation time spectra as slowing down of the fast mode and an increase of its amplitude. Further amounts of added water can be accommodated either in the interior of the already formed particles or by formation of new particles from the bilayer of the vesicles. The latter gradually disappear and simultaneously the former particles increase in size and eventually all bilayers are transformed into water-in-oil droplets stabilized by a monolayer of the copolymer located on the phase boundary (Figure 14c). Basically the same events take place during the solubilization of water in reverse disks which are formed by $(DDGG)_7(EO)_{45}(DDGG)_7$ in heptane.

In short, the bilayer structure of the reverse particles formed in heptane is not preserved upon water solubilization and the dispersions undergo transition to water-in-oil emulsions stabilized by a monolayer of the copolymer. The latter particles gradually increase in size from several to tens of nanometers. At high water contents the samples are transformed into unmeasurable milky-white opalescent dispersions which indicates large particles.

Closing Remarks and Implications for Some Applications

This contribution first examines the self-assembly in selective solvents of amphiphilic copolymers of EO and lipid-mimetic

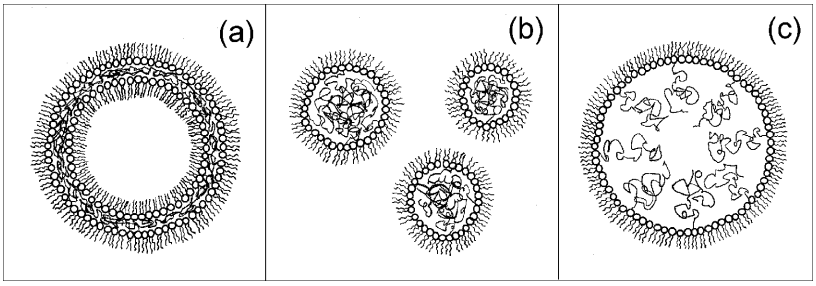

Figure 14. Schematic representation of structural changes in reverse vesicles of DDGG/EO copolymers formed in heptane upon water solubilization: (a) intact reverse vesicles; (b) reverse micellelike aggregates with PEG dominated cores; (c) copolymer stabilized water-in-oil emulsion droplets. The open circles with two narrow lines represent DDGG lipid-mimetic monomer units. The wider curved lines represent PEG chains that are covalently attached to the poly(DDGG) blocks. Structures are not drawn to scale.

oxirane, DDGG. The hydrophobic volume of the present copolymers was increased by increasing the degree of polymerization of DDGG and, in addition, the PEG headgroup size was decreased compared to related copolymers studied earlier.[17,18,26,36] The resulting change in the molecular geometry was sufficient for vesicle formation in aqueous solution as anticipated by simple shape considerations. The formation of vesicles from amphiphilic copolymers is not frequently observed; only a few research groups have reported investigations of polymer aggregates including vesicles.[60−64]

The vesicles of the EO/DDGG copolymers can be compared to PEG-stabilized liposomes. Both constituents of the latter, the lipid molecules and the PEG-lipids**,** can be rather mobile both within the bilayer and with respect to exchange via the aqueous phase with other bilayer structures, which may result in undesirable changes in the membrane properties and loss of the longevity. The large size of the EO/DDGG copolymers leads to slow kinetics and may be a factor that enhances the structural stability of the vesicles. The ether linkage and the lack of charge offer other advantages. As shown elsewhere,[65] the nonionic copolymers are less pH and saline sensitive than ionic surfactants. Furthermore, the ether linkage provides excellent stability against hydrolysis. Taken all these features together, enhancement of the chemical and structural stability as well as the circulation time of the vesicles can be anticipated, which makes them possible candidates for drug delivery.

The coexistence of unilamellar and multilamellar vesicles as well as vesicles with folded internal structures is notable. The latter two vesicle types have larger hydrophobic volume than the unilamellar vesicles. That may be why the vesicles of the present copolymers have a large capacity to solubilize heptane. The literature contains few studies providing information on solubilization of aliphatic compounds.[56,66−69] Predictions of solubilization capacity of Pluronic copolymers have been made on the basis of the theory of solubilization.[57] We observe that the experimental values determined for the present copolymers are consistently larger than those of Pluronic copolymers.

We demonstrate that the copolymers form reverse vesicles and disks in heptane, which is remarkable. Also, the reverse aggregates are obtained spontaneously, that is, without adding mechanical energy. Normally, reverse aggregates are produced in the presence of small amounts of water which enhance the surfactant self-assembly. However, no water is necessary for the self-assembly of the EO/DDGG copolymers in heptane. On the contrary, the addition of water to preformed reverse vesicles or disks is detrimental since it leads to transition to a nonbilayer phase. Nevertheless, the resulting water-in-oil emulsion particles are stable and able to solubilize more water. One could imagine employing these copolymers for delivery of hydrophilic active agents in nonaqueous media in addition to possible applications in processes of extraction and separation of hydrophilic substances.

No less notable is the ability of the copolymers to produce vesicles both in aqueous and nonaqueous solvents. During the vesicle formation a fraction of the surrounding medium is encapsulated, the total amount of which depends on the concentration, size, molecular weight, and structure of the vesicles. Calculations based on the LS data show that $(EO)_{45}$-$(DDGG)_8$ vesicles in heptane are able to entrap 3.4 vol. % of the solvent at the highest concentration studied. The corresponding figures in water are 1.4 and 2.8 vol. % for $(EO)_{45}$-$(DDGG)_8$ and $(DDGG)_7(EO)_{45}(DDGG)_7$, respectively. The lower values most probably reflect the presence of fractions of multilamellar vesicles or vesicles with internal lamellar structures. Despite this the solvent pools still constitute the major part of the particle volume which would allow encapsulation of both hydrophobic and hydrophilic compounds at a high agent-to-copolymer ratio.

In summary, both aqueous and nonaqueous dispersions of $(EO)_{45}(DDGG)_8$ and $(DDGG)_7(EO)_{45}(DDGG)_7$ exhibit a number of useful properties such as high structural and chemical stability, high solubilization capacity for substances that are insoluble in the surrounding media, and ability to entrap water-soluble and oil-soluble substances in the internal solvent pools.

Acknowledgment. Financial support from the Swedish Research Council and the Swedish Cancer Foundation is gratefully acknowledged. The synthetic part of the study was supported by the Bulgarian National Fund Scientific Research (Project X-808). We thank G. Karlsson for helping us with the electron microscopy.

References and Notes

(1) Bangham, A. D.; Hill, M. W.; Miller, N. G. A. In *Methods in Membrane Biology*; Korn, E. D., Eds.; Plenum: New York, 1974; Vol. 1, p 1.

(2) Cabanchik, Z. I.; Darmon, A. In *Structure and Properties of Cell Membranes*; Benga, G., Eds.; CRC Press: Boca Raton, 1985; Vol. III, p 123.

(3) Ostro, M. J. *Liposomes: From Biophysics to Therapeutics*; Dekker: New York, 1987.

(4) Sackmann, E.; Duwe, H.-P.; Engelhart, H. *Faraday Discuss. Chem. Soc.* **1986**, *81*, 281.

(5) Sackmann, E.; Duwe, H.-P.; Zeman, K.; Zilker, A. In *Structure and Dynamics of Nucleic Acids, Proteins and Membranes*; Clementi, E., Chin, S. Eds.; Plenum: New York, 1986.

(6) Almong, S.; Kushnir, T.; Nir, S.; Lichtenberg, D. *Biochemistry* **1986**, *25*, 2597.

(7) Schurtenberger, P.; Mazer, N. A.; Kanzig, W. *J. Phys. Chem.* **1985**, *89*, 1042.

(8) Aveldano, M. I. *Arch. Biochem. Biophys.* **1995**, *324*, 331.

(9) Jiang, S. S.; Fan, L. L.; Yang, S. J.; Kuo, S. Y.; Pan, R. L. *Arch. Biochem. Biophys.* **1997**, *346*, 105.

(10) Needham, D.; Hristova, K.; McIntosh, T.; Dewhirst, M.; Wu, N.; Lasic, D. *J Liposome Res.* **1992**, *2*, 411.
(11) Williams, S.; Alosco, T.; Mayhew, E.; Lasic, D.; Blankert, R. *Cancer Res.* **1993**, *53*, 3964.
(12) Uster, P. S.; Allen, T. M.; Daniel, B. E.; Mendez, C. J.; Newman, M. S.; Zhu, G. Z. *FEBS Lett.* **1996**, *386*, 243.
(13) Allen, T. M. *Curr. Opin. Colloid Interface Sci.* **1996**, *1*, 645.
(14) Johnsson, M.; Bergstrand, N.; Edwards, K. *J. Liposome Res.* **1999**, *9*, 53.
(15) Allen, T. M.; Hansen, C. B.; Lopes-de-Menezes, D. E. *Adv. Drug. Del. Rev.* **1995**, *16*, 267.
(16) Woodle, M. *Adv. Drug. Del. Rev.* **1995**, *16*, 249.
(17) Rangelov, S.; Edwards, K.; Almgren, M.; Karlsson, G. *Langmuir* **2003**, *19*, 172.
(18) Rangelov, S.; Almgren, M.; Tsvetanov, Ch.; Edwards, K. *Macromolecules* **2002**, *35*, 4770.
(19) Tartar, H. V. *J. Phys. Chem.* **1955**, *59*, 1195.
(20) Tanford, C. *J. Phys. Chem.* **1972**, *76*, 3020.
(21) Israelachvili, J. N.; Mitchel, J.; Ninham, B. W. *J. Chem. Soc., Faraday Trans. 2* **1976**, *72*, 1525.
(22) Lasic, D. D.; Woodle, M. C.; Martin, F. J.; Valentincic, T. *Period. Biol.* **1991**, *93*, 287.
(23) Trubetskoy, V. S.; Torchilin, V. P. *STP Pharma Sci.* **1996**, *6*, 79.
(24) Weissig, V.; Lizano, C.; Torchilin, V. P. *J. Liposome Res.* **1998**, *8*, 391.
(25) Johnsson, M.; Hansson, P.; Edwards, K. *J. Phys. Chem. B* **2001**, *105*, 8420.
(26) Rangelov, S.; Almgren, M.; Tsvetanov, Ch.; Edwards, K. *Macromolecules* **2002**, *35*, 7074.
(27) Kunieda, H.; Nakamura, K.; Evans, D. F. *J. Am. Chem. Soc.* **1991**, *113*, 1051.
(28) Kunieda, H.; Nakamura, K.; Davis, H. T.; Evans, D. F. *Langmuir* **1991**, *7*, 1915.
(29) Kunieda, H.; Yamagata, M. *J. Colloid Interface Sci.* **1992**, *150*, 277.
(30) Kunieda, H.; Makino, S.; Ushio, N. *J. Colloid Interface Sci.* **1992**, *147*, 286.
(31) Kunieda, H.; Nakamura, K.; Infante, M. R.; Solans, C. *Adv. Mater.* **1992**, *4*, 291.
(32) Kunieda, H.; Nakamura, K.; Olsson, U.; Lindman, B. *J. Phys. Chem.* **1993**, *97*, 9525.
(33) Nakamura, K.; Uemoto, A.; Imae, T.; Solans, C.; Kunieda, H. *J. Colloid Interface Sci.* **1995**, *170*, 367.
(34) Kunieda, H.; Kanei, N.; Uemoto, A.; Tobita, I. *Langmuir* **1994**, *10*, 4006.
(35) Ebbing, M. H. K.; Villa, M.-J.; Valpuesta, J.-M.; Prados, P.; de Mendoza, J. *Proc. Natl. Acad. Sci. U.S.A.* **2002**, *99*, 4962.
(36) Rangelov, S.; Petrova, E.; Berlinova, I.; Tsvetanov, Ch. *Polymer* **2001**, *42*, 4483.
(37) Fendler, J. *Membrane Mimetic Chemistry*; John Wiley & Sons: New York, 1982.
(38) Hope, M. J.; Bally, M. B.; Webb, G.; Cullis, P. R. *Biochim. Biophys. Acta* **1985**, *812*, 55.
(39) New, R. R. C. In *Liposomes as Tools in Basic Research and Industry*; Philippot, J. R., Schuber, F., Eds.; CRC Press: Boca Raton, FL, 1995.
(40) Rangelov, S.; Brown, W. *Polymer* **2000**, *41*, 4825.
(41) Chu, B. *Laser Light Scattering, 2*; Academic Press: New York, 1991.
(42) Jakes, J. *Czech. J. Phys. B* **1988**, *38*, 1305.
(43) Talmon, Y. *Ber. Bunsen-Ges. Phys. Chem.* **1996**, *100*, 364.
(44) Almgren, M.; Edwards, K.; Gustafsson, J. *Curr. Opin. Colloid Interface Sci.* **1996**, *1*, 270.
(45) Burchard, W.; Richtering, W. *Prog. Colloid Polym. Sci.* **1989**, *80*, 151.
(46) Burchard, W. *Adv. Polym. Sci.* **1983**, *48*, 1.
(47) Isihara, A.; Hayashida, T. *J. Phys. Soc. Jpn.* **1951**, *6*, 40.
(48) Isihara, A.; Hayashida, T. *J. Phys. Soc. Jpn.* **1951**, *6*, 46.
(49) Yamakawa, H. *Modern Theory of Polymer Solutions*; Harpers and Row: New York, 1971.
(50) Yamakawa, H.; Fujii, M. *Macromolecules* **1973**, *6*, 407.
(51) Mazer, N. A.; Benedek, G. B.; Carey, M. C. *Biochemistry* **1980**, *19*, 601.
(52) Hansen, J. P.; McDonald, I. R. *Theory of Simple Liqiuds*, 2nd ed.; Academic Press: London, 1986.
(53) Schurtenberger, P.; Newman, M. E. In *Environmental Particles*; Buffle, J., van Leeuwen, H. P, Eds.; Lewis Publishers: Boca Raton, FL, 1993; Vol. 2; p 37.
(54) Egelhaaf, S.; Schurtenberger, P. *J. Phys. Chem.* **1994**, *98*, 8560.
(55) Tanford, C. *The Hydrophobic Effect: Formation of Micelles and Biological Membranes*; John Wiley & Sons: New York, 1973.
(56) Nagarajan, R.; Barry, M.; Ruckenstein, E. *Langmuir* **1986**, *1*, 210.
(57) Nagarajan, R. *Colloids Surf. B: Biointerfaces* **1999**, *16*, 55.
(58) Nagle, J. F.; Tristram-Nagle, S. *Biochim. Biophys. Acta* **2000**, *1469*, 159.
(59) Stepanek, P. *J. Chem. Phys.* **1993**, *99*, 6384.
(60) Discher, B. M.; Won, Y. Y.; Ege, D. S.; Lee, J. C.-M.; Bates, F. S.; Discher, D. E.; Hammer, D. A. *Science* **1999**, *284*, 1143.
(61) Laibin, L.; Eisenberg, A. *J. Am. Chem. Soc.* **2001**, *123*, 1012.
(62) Harris, J. K.; Rose, G. D.; Bruening, M. L. *Langmuir* **2002**, *18*, 5337.
(63) Won, Y. Y.; Brannan, A. K.; Davis, H. T.; Bates, F. S. *J. Phys. Chem. B* **2002**, *106*, 3354.
(64) Choucair, A. A.; Kycia, A. H.; Eisenberg, A. *Langmuir* **2003**, *19*, 1001.
(65) Rosen, M. J. *Surfactants and Interfacial Phenomena*; Wiley-Interscience: New York, 1989; pp 21−23.
(66) Kabanov, A. V.; Nazarova, I. R.; Astafieva, I. V.; Batrakova, E. V.; Alakhov, V. Yu.; Yaroslavov, A. A.; Kabanov, V. A. *Macromolecules* **1995**, *28*, 2303.
(67) Gadelle, F.; Koros, W. J.; Schechter, R. S. *Macromolecules* **1995**, *28*, 4883.
(68) Wu, G.; Chu, B.; Schneider, D. K. *J. Phys. Chem.* **1995**, *99*, 5094.
(69) Tian, M.; Arca, E.; Tuzar, Z.; Webber, S. E.; Munk, P. *J. Polym. Sci., Part B: Polym. Phys.* **1995**, *33*, 1713.